


Article

Study of the Critical Safe Height of Goaf in Underground Metal Mines

Qinli Zhang ¹, Peng Zhang ¹ , Qiusong Chen ^{1,*}, Hongpeng Li ², Zian Song ¹ and Yunbo Tao ¹

¹ School of Resources and Safety Engineering, Central South University, Changsha 410083, China; zhangqinlicn@126.com (Q.Z.); 215512116@csu.edu.cn (P.Z.); 225512120@csu.edu.cn (Z.S.); yunbo.tao@csu.edu.cn (Y.T.)

² Jiangxi Copper Industry Group Yinshan Mining Industry Co., Ltd., Shangrao 334200, China; lihongpeng2024@163.com

* Correspondence: qiusong.chen@csu.edu.cn; Tel.: +86-199-1150-0066

Abstract: The empty-space subsequent filling mining method is the main mining scheme for underground metal mines to achieve large-scale mechanized mining. The stage height, one of the main parameters of this method, affects the various production process aspects of the mine and influences the stability of the goaf. In order to determine the stage height scientifically and rationally in the empty-space subsequent filling mining method, a formula for the stabilized critical safe height of a high goaf in an underground metal mine was derived based on Pu's arch equilibrium theory, Bieniawski's pillar strength limit theory, and the Kastner equation and combined with the results of an orthogonal analysis to rank the importance of the main factors in the formula. A copper mine in Jiangxi Province was used as a case study, with the reliability of the formula verified by numerical simulation and industrial testing. The factors in the formula influencing the critical stabilized safe height of the goaf were, in descending order, the compressive strength of the rock body, the width of the two-step mining pillar, the width of the one-step mining room, the mining height, and the depth of mining. Based on the calculation results, the recommended stage heights are 30 m (−378 m middle section) and 25 m (−478 m middle section) in the area of poor rock body stability and 50 m in the area of better rock body stability. The simulation results show that the goaf is significantly affected by the compressive stress under the condition of a certain rock body stability and that the compressive stress increases with increasing goaf height. The minimum recommended values of the sidewall safety coefficients in areas of poor and better rock stability are 1.04 and 1.06, respectively. The volume deviation coefficients of the three industrial test mines were all controlled within 3%, indicating that no obvious collapse and destabilization phenomenon occurred in the goaf. This paper provides some theoretical and applied guidance for the stage height design of similar underground metal mines using the empty-space subsequent filling mining method.

Keywords: critical height of goaf; the empty-space subsequent filling mining method; rock stability; numerical simulation; industrial tests



Citation: Zhang, Q.; Zhang, P.; Chen, Q.; Li, H.; Song, Z.; Tao, Y. Study of the Critical Safe Height of Goaf in Underground Metal Mines. *Minerals* **2024**, *14*, 227. <https://doi.org/10.3390/min14030227>

Academic Editor: Abbas Taheri

Received: 19 January 2024

Revised: 19 February 2024

Accepted: 22 February 2024

Published: 23 February 2024



Copyright: © 2024 by the authors. Licensee MDPI, Basel, Switzerland. This article is an open access article distributed under the terms and conditions of the Creative Commons Attribution (CC BY) license (<https://creativecommons.org/licenses/by/4.0/>).

1. Introduction

In underground metal mining, the empty-space subsequent filling mining method has become one of the main mining schemes because of its advantages of high production capacity, low cost, high recovery rate, and protection of underground and surface environments [1–7]. The empty-space subsequent filling mining method, whether it is staged open-field subsequent filling or segmented open-field subsequent filling, generally divides the ore block into a one-step mining room and a two-step ore pillar during the mining process and carries out the mining in two steps. After the completion of stoping, the stage height of the goaf can reach tens or even hundreds of meters. Once the goaf height becomes unstable, it poses a threat to the equipment and personnel involved in

underground production and increases the difficulty of mining in adjacent areas, resulting in resource waste [8–10].

Many hydrogeological, rock stress-strain behavior, geometric, and engineering factors affect the safe proportions of goaf [11–15]. Extensive research has been conducted on the ultimate exposed area and ultimate span of the goaf roof in underground mining. Based on a summary of numerous mining engineering practices, Matthews proposed a diagrammatic method for assessing the relationship between the stability index N of a rock mass and the shape coefficient of the exposed mining area [16]. Jang et al. proposed a stability stress mechanics model for goaf and discussed the relationship between the ultimate exposed area of goaf and the span ratio, joint density of the fracture surface, and joint diameter [17]. Swift et al. used an elastic beam model and a pillar strength formula to study the relationship between the exposed area of goaf, the pillar stability, and a safety factor [18]. Gao et al. simulated the distribution and variation patterns of stress, displacement, and the plastic zone in goaf for different span ratios using the PLAXIS 2D finite element analysis software [19]. Zhienbayev, A. et al. performed the calculations, modelling, and statistic analysis of factual rock falls from the roof to ensure the roof span stability in terms of room-and-pillar system of mining [20]. Hosseini, M. et al. conducted a sensitivity analysis using the numerical, squat pillar, and Mathews stability methods through the Taguchi technique to properly understand the influence of geometric parameters and stress on stope stability according to Sormeh underground mine data [21]. Although the ultimate exposed area and ultimate span of the goaf roof have been studied extensively, the influence of goaf height on goaf stability has not been adequately examined.

Bagde evaluated the impact of mining height on the stability of goaf through empirical methods, numerical simulations, and on-site rock deformation monitoring [22]. Soni et al. used numerical simulation to study the variation of pillar strength with height during the implementation of the room-and-pillar mining method in mines [23]. Zhang et al. used an orthogonal experimental design method to investigate the effects of the height, length, and width of mining pillars and the length and width of mining rooms on the stability of goaf [24]. Qiu et al. derived a limit equilibrium equation for mining pillars based on the area-bearing theory and used this equation to optimize the structural parameters of the mining area, such as the mining height, pillar spacing, and row spacing [25]. The research results obtained to date are of great significance in optimizing the mining height using the room column method. However, there has been relatively little research on the stability of high goaf using the subsequent filling mining method. Research on the safe critical height for maintaining self-stability in high goaf is still at an early stage.

A copper mine in Jiangxi was taken as a case study in this research to examine this issue. Using Bieniawski's ultimate pillar strength theory [26], Pu's arch equilibrium theory [27], and the Kastner equation [28], a formula was derived for the critical stable height of goaf. A sensitivity analysis of the factors affecting the critical safe height of goaf was conducted using the orthogonal range analysis method. On the basis of rock mechanics experiments and reduction of rock mechanics parameters, the critical safe height of the goaf of the copper mine was calculated. The value obtained was verified through numerical simulation analysis and on-site experiments. The research results provide a theoretical basis and engineering reference for designing reasonable mining stage heights for similar underground metal mines under various geological and mining conditions.

2. Methods

2.1. Study Site

The Jiangxi copper mine is located in Shangrao City, Jiangxi Province. The mine area is about 2.7 km long from north to south and 2.5 km wide from east to west, covering an area of about 6.75 km². The average surface elevation of the mine is +50 m, and the elevations of the first and second mining sections are −308 m to −378 m and −408 m to −478 m, respectively. There are a total of 11 large ore bodies in the copper–sulfur–gold section, with S1, N1, N2, and N3 being the main ore bodies. The dip of the ore body ranges from 76°

to 88° , with an average of 83° ; the ore body mainly strikes EW-NEE, S dips; distributed between exploration lines 03 and 14; and the length of the ore body along the strike ranges from 700 to 1300 m; the thickness of the single project ranges from 1.00 m to 66.70 m, with an average true thickness of 12.5 m. The ore body mainly exists in the contact zone with altered phyllite, with a small amount occurring in blast breccia, altered quartz diorite, and quartz porphyry. Tectonic development of folds and fractures results in poor stability of the ore rocks. The empty-space subsequent filling mining method is the main mining method used in the mine, accounting for 66% of the total. Mining is conducted in intervals. The current mining structure parameters used in the mine have poor compatibility with geological and mining conditions, resulting in frequent collapse events of the one-step mining room during the mining process.

2.2. Experiments Rock Mechanics Parameter and Their Reduction

The rock samples were taken from the underground mining stope of a lead-zinc copper mine in Jiangxi Province. In accordance with the requirements of the rock mechanics parameter experiments, the specimens were drilled using a rock drilling core machine with a diameter of $\varphi = 50$ mm. The specimen is cut and sanded into a cylindrical shape. For uniaxial and triaxial compression tests, the recommended ratio of specimen height to diameter is 2:1, which is 100 mm in height and 50 mm in diameter. The actual error is controlled within ± 3 mm. For the Brazilian splitting test, the ratio of specimen height to diameter is controlled at 1:1. The actual error is controlled within ± 2 mm.

Rock mechanical parameter experiments were conducted using MTS 322 rock mechanical press and MTS 815 rock mechanical press. The experiment was conducted using the transverse isobaric triaxial method at room temperatures in the range of $24\text{--}28^\circ\text{C}$ and 55%–79% relative humidity. The displacement loading method was used to maintain a loading rate of 0.045 mm/min throughout the experiment. The loading process stops automatically when the maximum load is reached and the specimen fails.

Since the rock strength obtained from the indoor tests is actually the rock strength of the intact rock mass, it differs significantly from the rock strength in the field. Therefore, it is necessary to discount its strength. The empirical discounting method has the advantages of being simple to apply and dealing effectively with some uncertain factors. It has become the most important method for studying the strength parameters of rock masses. The Hoek–Brown strength criterion for discounting the strength of a rock mass based on certain indoor and field test data has become the most commonly used discounting method. Empirical formulas for discounting the strength of the rock mass based on the geological description of the rock mass in the field and the statistical data from the investigation of the joints and fractures on the structural surface are considered.

2.3. Theoretical Modelling

After excavation of the rock mass, the stresses in the rock mass are redistributed. The pillar is pressurized by the overlying rock layer, and the top rock layer shows large compressive deformation, forming a small pressure-free arch. It is worth noting that once formed, the pressure-free arch will not disappear with the backfilling of the mining space and is an irreversible deformation phenomenon. Therefore, the smaller pressure-free arches above adjacent spaces gradually merge to form a large pressure-free arch. As shown in Figure 1, a plastic zone with radius R_p will be formed above the goaf. The size of the plastic zone is not only related to the nature of the rock body and the structural parameters of the stope, but is also affected by the mining burial depth. The load on the pillar is the self-weight of the rock body within the plastic zone above its roof. As long as the pillar can withstand the gravity of the rock body within the plastic zone of the top plate surrounding the rock, the long-term stability of the pillar can be ensured.

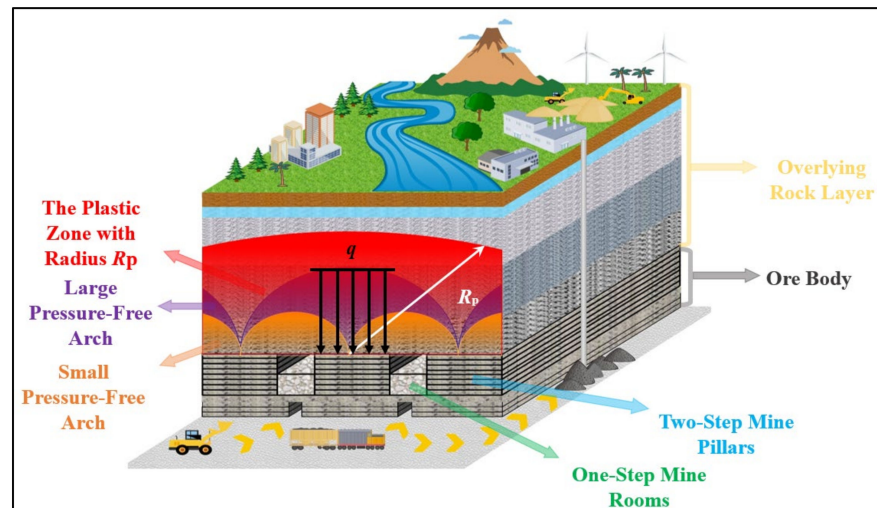


Figure 1. Theoretical modelling of the critical safe height of goaf.

According to the bearing mechanism of the pillar, the load carried by the pillar is the self-weight of all the rock bodies within the plastic zone above its roof. The radius of the plastic zone can be solved using the Kastner equation:

$$R_p = R_0 \left[\frac{(P_0 + c \cdot \cot \varphi)(1 - \sin \varphi)}{c \cdot \cot \varphi} \right]^{\frac{1 - \sin \varphi}{2 \sin \varphi}} \quad (1)$$

where R_p is the radius of the plastic zone, m; R_0 is the radius of excavation, m; P_0 is the vertical self-weight stress at the excavation, MPa, $P_0 = \gamma H$; c is the cohesive force of the rock mass, MPa; φ is the angle of internal friction of the rock mass, °; γ is the capacitance of the top plate surrounding rock, kN/m³; and H is the mining depth, m.

In order to ensure the stability of the pillar, the maximum range is used to calculate the roof pressure of the stope. Practice has shown that the radius of the plastic zone is less affected by the shape of the excavation section. Therefore, the excavation radius in the calculation is replaced by the equivalent excavation radius—that is, the radius of the external circle with different shapes is used instead. The excavation radius R_0 can be expressed as follows:

$$R_0 = \sqrt{\left(\frac{L}{2}\right)^2 + \left(\frac{H_1}{2}\right)^2} \quad (2)$$

where L is the mining space span, m, and H_1 is the height of the mining pillar, m.

The principle of calculating a rectangular mining pillar is shown in Figure 1. According to the theory of area-bearing capacity, the bearing capacity of a mining pillar is the gravity of the rock body in the overlying plastic zone, and the area of bearing is the sum of the area of the pillar itself and the mining area apportioned by the pillar, so that the following equilibrium equations can be obtained:

$$\sigma_p W_p L_p = (W_0 + W_p) L_p P_{zz} \quad (3)$$

where σ_p is the axial average stress of the ore column, MPa; P_{zz} is the vertical stress in the thickness of the plastic zone of the overlying rock layer, MPa; W_0 the width of the mining room, m; W_p the width of the mine pillar, m; L_p the length of the stope, m.

Knowing that $P_{zz} = \gamma R_p$ and substituting it into the above equation, the average axial stress of the ore column can be obtained as follows:

$$\sigma_p = \frac{(W_0 + W_p) \gamma R_0 \left[\frac{(\gamma H + c \cdot \cos \varphi)(1 - \sin \varphi)}{c \cdot \cot \varphi} \right]^{\frac{1 - \sin \varphi}{2 \sin \varphi}}}{W_p} \quad (4)$$

The bearing strength of the pillar depends mainly on the compressive strength of the rock body (obtained by discounting based on the uniaxial compressive strength of the rock) and is related to the shape and width of the pillar. Researchers have proposed a variety of theoretical and empirical formulas for the bearing strength of mining pillars. The Bieniawski strength formula for mining pillars is one of the more widely used. In this study, the Bieniawski formula was used to calculate the strength of the mine pillar as follows:

$$S_p = \sigma_c \left[0.64 + 0.36 \left(\frac{W_p}{h} \right)^\alpha \right] \quad (5)$$

where S_p is the strength of the ore column, MPa; σ_c is the average compressive strength of the ore column, MPa; h is the height of the ore column, m; α is a constant = 1.0 when the width-to-height ratio of the ore column is less than 5 and 1.4 when the width-to-height ratio of the ore column is greater than 5.

In order to simplify the problem, only the main influences that can be quantified are considered. From Equations (4) and (5), a factor of safety can be derived for rectangular pillars, $K = \sigma_p / S_p$. When $K > 1$, the ore column is in a stable state; when $K < 1$, the ore column is in an unstable state; when $K = 1$, the ore column is in a critical state. When the column is in the critical state, the critical height of the column instability meets the relationship equation:

$$h = \alpha \sqrt{\frac{\sigma_c W_p (0.36 W_p)^\alpha}{(W_0 + W_p) \gamma R_0 \left[\frac{(\gamma H + c \cot \varphi)(1 - \sin \varphi)}{c \cot \varphi} \right]^{\frac{1 - \sin \varphi}{2 \sin \varphi}} - 0.64 \sigma_c W_p}} \quad (6)$$

2.4. Numerical Simulation Tests

FLAC 3D (Fast Lagrangian Analysis of Continua) uses the “Explicit Lagrangian” algorithm and the “Hybrid-Discrete Partitioning” technique to simulate the plastic damage and flow of materials very accurately. It has a good pre-processing function. When calculating, the program automatically dissects the model into hexahedral cells, and each cell can have its own material model, and the material can be yielded and flowed under the action of external force and stress field. Its post-processing functions are also very powerful. Users can print or plot their own data or graphs with the appropriate commands according to their needs. Therefore, FLAC 3D is one of the most ideal tools for solving the goaf stability problem. In this study, the software was used to simulate and analyze the safety critical heights of the goaf. In addition, the stability of the mining pillars is also discriminated using the Mohr-Coulomb strength criterion [29,30]. The principal stress is the main parameter of rock mechanics after discounting, and its relation is as follows [31,32]:

$$\sigma_3 = \sigma_1 \tan^2 \left(45^\circ - \frac{\varphi}{2} \right) - 2c \cdot \tan \left(45^\circ - \frac{\varphi}{2} \right) \quad (7)$$

$$f = \frac{\sigma_3}{\sigma_1} \quad (8)$$

2.4.1. Modeling

The model created in Rhino 6.0 was meshed and imported into Flac 3D, as shown in Figure 2. The length of the model along the strike of the ore body was set to 300 m, the length and width of the one-step mining room were 50 m and 12 m, respectively, and the length and width of the two-step mining pillar were 50 m and 18 m, respectively. To minimize the influence of the boundary conditions on the stresses in the mining operation area, the left and right sides of the back-mining area were enlarged by 150 m of bedrock to ensure that the boundary conditions were applied to the bedrock and were transmitted to the mining area through the bedrock. The height of the model was set to 800 m, and the average thickness of bedrock at the top was set to 400 m to avoid the top self-gravitating

stress acting directly on the goaf. The average thickness of bedrock at the bottom was set to 400 m to avoid the bottom boundary condition acting directly on the mining area, which would have caused stress concentration.

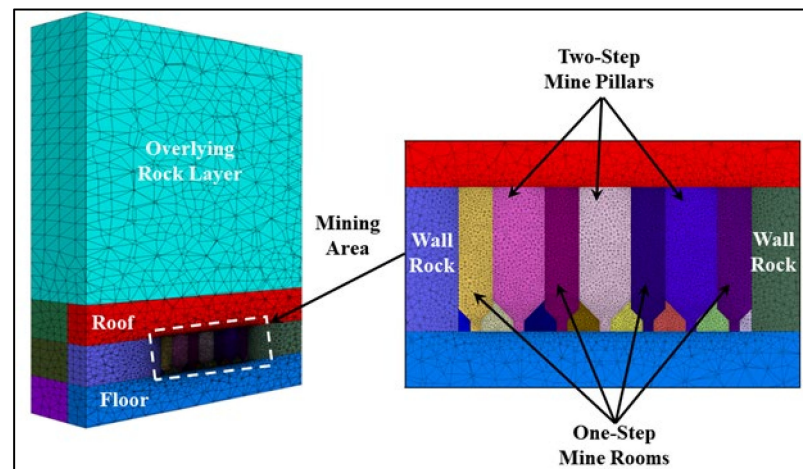


Figure 2. Numerical modeling of the critical safe height of goaf.

Based on the hosting conditions of the ore body, the model boundary was constrained from horizontal displacement, i.e., the boundary displacements in the x and y directions were zero.

2.4.2. Basic Assumption

In view of the complexity and variability of the actual engineering geological environment of the mine and the characteristics of the ore body endowment, the following assumptions need to be made in the numerical simulation process:

- (1) The horizontal thickness and inclination of the excavated ore body are fixed values;
- (2) The ore body is assumed to be an ideal elastic-plastic body, and the strength and volume of the material do not change with plastic deformation after the yield point;
- (3) The ore body and peripheral rock are locally homogeneous and isotropic materials, and plastic deformation does not change the material isotropy;
- (4) Considering the brittleness of the rock, all physical quantities involved in the analysis are independent of time;
- (5) Strain hardening (or softening) is not considered;
- (6) The sides of the model limit horizontal displacements and the bottom limits vertical displacements;
- (7) Considering the limitations of the finite element program, it is assumed that there is no influence of tectonic activities in the site, the original rock ground stress is of geostrophic field type, there is an integrated contact between the rock layers, the interior of the rock layer is a continuous medium, the influence of groundwater activities is not taken into account in the model, and the existence and influence of structural surfaces, fissures, and weak layers in the rock layer and ore body are not taken into account;
- (8) The loads selected for the calculations will not change with the orientation of the units, but will always maintain their original orientation, with the surface loads acting normal to the surface of the deformed units and can be used to simulate “following” forces, the magnitude of which is the weight of the overlying rock formation;
- (9) Simulation of the most hazardous scenario, i.e., mining in intervals.

2.4.3. Parameters

Based on the numerical simulation test scheme shown in Table 1, combined with the results of the rock body mechanical parameter discounting in Table 3 in Section 3.1, the

corresponding mechanical parameters were set for the overlying rock layer, the ore body, and the bottom plate of the model.

Table 1. Test Programs.

Program Number	Rock Stability	Compressive Strength (σ_t /MPa)	Width of the Stope		Length of the Stope (m)	Height of the Stope (m)
			One-Step Mine Room (m)	Two-Step Mine Pillar (m)		
1	Poor	10.93	12	18	50	25
2	Poor	10.93	12	18	50	30
3	Poor	10.93	12	18	50	35
4	Better	22.97	12	18	50	45
5	Better	22.97	12	18	50	50
6	Better	22.97	12	18	50	55

2.4.4. Simulation Schemes

The two-step mining process was used to analyze the critical height of the pillar instability for the two types of areas with better and worse surrounding rock stability. The length and width parameters of the one-step mining room and the two-step pillar were unchanged; only the mining height of the stope was changed. Parameterization of the mining height in the field of values in the vicinity of the theoretically calculated values of the critical safe height of stope in different stability area was conducted. The specific parameters of the mining height are shown in Table 1.

3. Results and Discussion

3.1. Results of Experiments Rock Mechanics Parameter and Their Reduction

Comparison of the results in Tables 2 and 3 reflects that:

Table 2. Experiment results of rock mechanical parameters.

Materials	Compressive Strength (σ_t /MPa)	Tensile Strength (σ_c /Mpa)	Elasticity Modulus (E_m /Gpa)	Density ($\rho/t \cdot m^{-3}$)	Poisson's Ratio (μ)	Cohesion (C_m /Mpa)	Internal Friction Angle ($\varphi_m/^\circ$)
Overburden Rock	68.54	8.89	39.29	2.84	0.24	10.31	50.41
Phyllite ore body	33.80	6.28	27.40	2.97	0.34	3.33	43.39
Floor	46.69	6.05	24.63	2.88	0.32	7.14	50.43

Table 3. Summary of discounted rock mechanics parameters results of rock mechanical parameters.

Materials	Compressive Strength (σ_t /Mpa)	Tensile Strength (σ_c /Mpa)	Elasticity Modulus (E_m /Gpa)	Density ($\rho/t \cdot m^{-3}$)	Poisson's Ratio (μ)	Cohesion (C_m /Mpa)	Internal Friction Angle ($\varphi_m/^\circ$)
Overburden Rock	29.99	3.89	25.25	2.84	0.24	10.31	50.41
Phyllite ore body (better)	22.97	4.27	24.64	2970	0.34	3.33	43.39
Phyllite ore body (poor)	10.93	2.03	9.69	2970	0.34	3.33	43.39
Floor	18.23	3.75	20.69	2880	0.32	7.14	50.43

The gap between the mechanical strength of rocks before and after discounting is significant. For example, the compressive strength, tensile strength, and elasticity modulus of the Overburden rock are 68.54 Mpa, 8.89 Mpa, and 39.29 Gpa before reduction, and 22.99 Mpa, 3.89 Mpa, and 25.25 Gpa after reduction.

The gap between the same kind of rocks in the areas with different stability is significant after reduction. For example, the compressive strength, tensile strength, and elasticity modulus of the Phyllite ore body are 22.97 Mpa, 4.27 Mpa, and 24.64 Gpa, respectively, in the region with good stability, and 10.93 Mpa, 2.03 Mpa, and 9.69 Gpa, respectively, in the region with poor stability.

Other rock mechanical parameters remain unchanged before and after the reduction.

3.2. Quantitative Analysis of Each Influencing Factor

The analysis of the critical safe height of the goaf showed that the factors affecting the stability of the goaf were the rock body compressive strength, mine room width, pillar width, mining height, bearing capacity of the overlying rock layer, mining depth, and mining radius. Together with the geological conditions and mining technology conditions of the mine, the main influencing factors were identified as the rock body compressive strength, mine room width, mine pillar width, mining height, and mining depth. The sensitivity of each of these factors was analyzed quantitatively using orthogonal extreme difference analysis. The values of the main influencing factors were established in the range of five-factor, five-level-structure orthogonal tests. Table 4 lists the parameters of the critical safe height of the goaf and the results of the orthogonal experiments.

Table 4. Parameters and results of orthogonal experiments.

Number of Tests	Mining Depth (m)	Compressive Strength (MPa)	Width of Mining Room (m)	Width of Mining Pillar (m)	Height of Stope (m)	Critical Height for Pillar Destabilization (m)
1	300	11	10	12	20	20.7
2	300	12	12	14	30	32.1
3	300	13	14	16	40	43.7
4	300	14	16	18	50	55.4
5	300	15	18	20	60	67.2
6	400	11	10	16	50	33.7
7	400	12	12	18	60	45.1
8	400	13	14	20	20	67.7
9	400	14	16	12	30	44.9
10	400	15	18	14	40	16.0
11	500	11	10	20	30	57.3
12	500	12	12	12	40	49.6
13	500	13	14	14	50	39.5
14	500	14	16	16	60	17.1
15	500	15	18	18	20	31.6
16	600	11	10	14	60	42.8
17	600	12	12	16	20	66.6
18	600	13	14	18	30	22.4
19	600	14	16	20	40	33.7
20	600	15	18	12	50	23.5
21	700	11	10	18	40	71.2
25	700	12	12	20	50	23.5
h_1	42.02	43.82	45.14	19.94	31.4	
h_2	40.04	41.48	43.38	29.88	32.68	
h_3	37.16	39.02	38.32	40.52	40.82	
h_4	35.84	37.8	36.82	51.7	45.14	
h_5	36.24	37.8	36.26	57.88	49.88	
R	6.02	8.88	37.94	18.48	8.80	

Based on the results of the orthogonal experiment polar analysis shown in Table 4, the extreme difference R of the rock body discounted compressive strength, and the width of the pillar were 37.94 m and 18.48 m, respectively. The extreme difference of the width of the mine room, the height of the stope, and the depth of the mining were 8.88 m, 8.80 m, and 6.02 m, respectively. The results show that the critical height of the pillar instability in this copper mine results in the most significant factor being the rock body discounted compressive strength, followed by the width of the pillar, the width of the mine room, and the height of the stope. It is worth noting that the width of the mine room and the height of the stope have almost the same level of influence on the critical height of pillar instability. Therefore, the structural parameters of the stope should be adjusted according to the geological conditions of the mine in the process of ore body recovery. The width of the ore column should be increased as much as possible to ensure that the critical height of the ore column instability is greater than the height of the stope while ensuring the maximum width permitted for the limited exposure area of the empty area and the minimum width permitted for the self-supporting height of the filling body of the one-step stope.

One factor at a time was studied to analyze the quantitative relationship between the critical safe height of the goaf and the main influencing factors. Four model forms, a linear function, exponential function, power function, and logarithmic function, were used for fitting. The initial values of each influencing factor were set as follows: $\gamma = 2.97 \text{ kN}\cdot\text{m}^{-3}$, $H = 400 \text{ m}$, $W_0 = 12 \text{ m}$, $W_p = 18 \text{ m}$, $\sigma_c = 10.93 \text{ MPa}$, $C = 3.33 \text{ MPa}$, $L = 3(W_0 + W_p) = 90 \text{ m}$, $H_1 = 50 \text{ m}$, and $\varphi = 43.39^\circ$. The fitting results are shown in Table 5.

Table 5. Functional Relationship Fitting Results.

Main Influencing Factors	Fitting Methods	Fitting Formula	Correlation Coefficient
Depth of Mining	Linear Function	$y = -0.0097x + 29.91$	0.98279
	Exponential Function	$y = 30.3933e^{-0.0004x}$	0.98896
	Power Function	$y = 77.0907x^{-0.1823}$	0.99827
	Logarithmic Function	$y = 56.9144 - 5.0834 \ln(x + 45.6918)$	0.99976
Width of Mine Room	Linear Function	$y = -1.42x + 43.0000$	0.99683
	Exponential Function	$y = 51.9860 \times 0.9436^x$	0.99962
	Power Function	$y = 163.8241x^{-0.7431}$	0.99853
	Logarithmic Function	$y = 68.4447 - 17.482 \ln(x - 0.5964)$	0.99983
Compressive Strength	Linear Function	$y = 2.404x - 1.06$	0.98682
	Exponential Function	$y = 15.7814e^{0.0514x}$	0.98707
	Power Function	$y = 2.0802x^{1.0394}$	0.98765
	Logarithmic Function	$y = -14343.2765 + 2228.6499 \ln(x + 611.5214)$	0.87614
Width of Mine Pillar	Linear Function	$y = 1.45x - 0.3$	0.99778
	Exponential Function	$y = 8.27504 \times 1.0646^x$	0.98247
	Power Function	$y = 1.3922x^{1.0099}$	0.99769
	Logarithmic Function	$y = -119.4666 + 42.2206 \ln(x - 13.2732)$	0.99999
Height of the Stope	Linear Function	$y = -0.108x + 31.24$	0.98822
	Exponential Function	$y = 31.5312e^{-0.0039x}$	0.98161
	Power Function	$y = 44.4409x^{-0.1389}$	0.90038
	Logarithmic Function	$y = 755.4333 + 105.7652 \ln(x + 940.5610)$	0.98000

1. The highest correlation coefficient for the function fit between the mining depth and the critical safe height of the goaf was 0.99976 for the logarithmic function fit, i.e., it follows the decreasing law of the logarithmic function $y = a_1 + b_1 \ln(x + c_1)$ (in which a_1 , b_1 , and c_1 mainly depend on the mining depth, the rock body compressive strength, and other factors). Figure 3a shows the logarithmic function of the mining depth and the critical safe height of the goaf fitting curve. With increasing mining

depth, the critical safety height of the goaf followed a logarithmic function with the rate of reduction gradually decreasing.

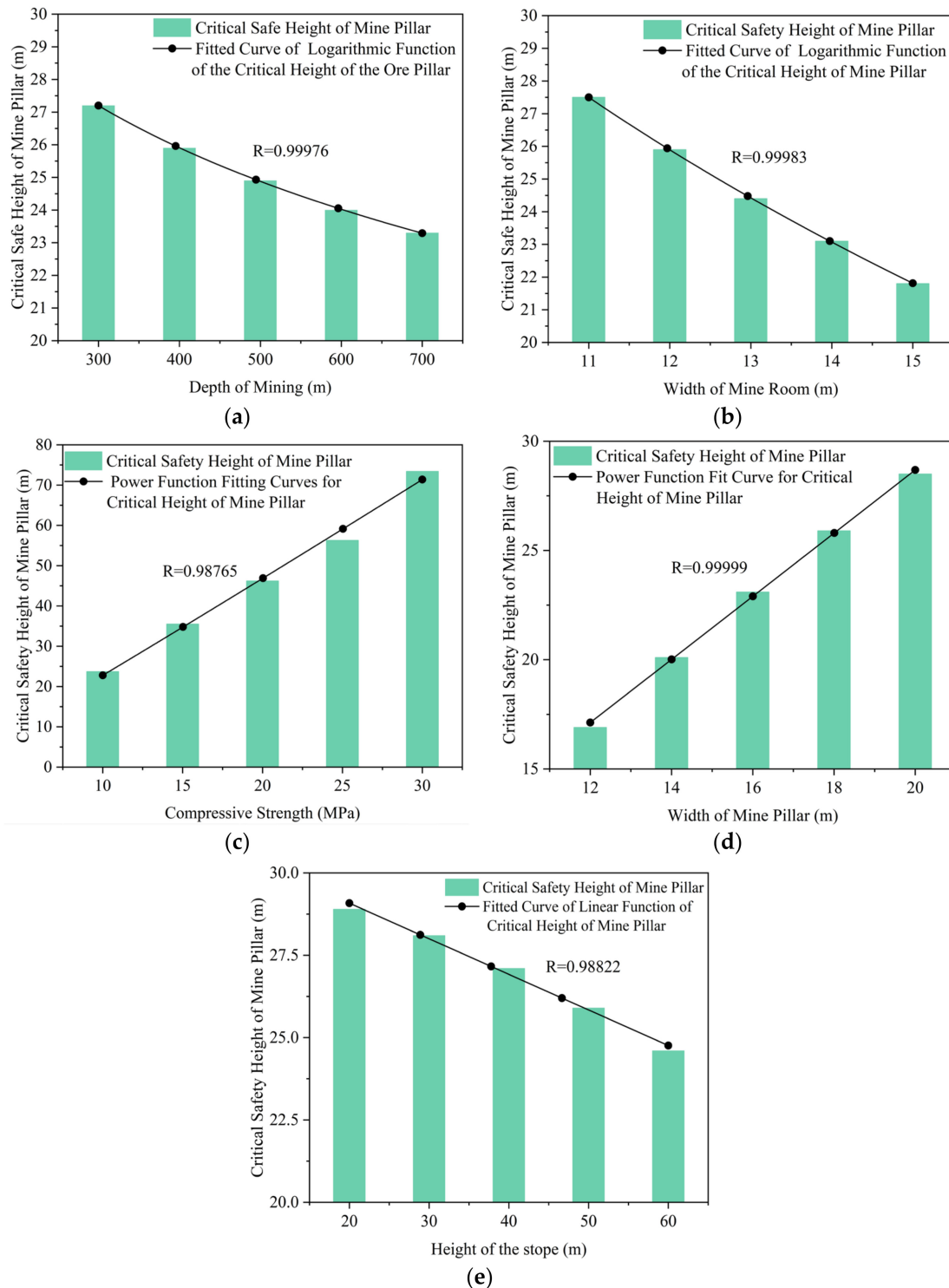


Figure 3. Function fitting curve. (a) Fitted curve of the logarithmic function of the critical safe height of mine pillar and the mining depth; (b) Fitted curve of the logarithmic function of the critical safe height of mine and the width of mine room; (c) Fitted curve of the logarithmic function of the critical safety height of mine pillar and the compressive strength of the rock body; (d) Fitted curve of the logarithmic function of the critical safe height of mine pillar and the width of mine pillar; (e) Fitted curve of logarithmic function of the critical safe height of mine pillar and the height of slope.

2. The highest correlation coefficient between the width of the mining room and the critical safety height of the goaf function fit was the logarithmic function fit of 0.99983, that is, following a logarithmic function of the form $y = a_2 - b_2 \ln(x + c_2)$, where a_2 , b_2 , and c_2 mainly depend on the width of the mining room, the rock body compressive strength, and other factors. Figure 3b shows the fitting curve of the logarithmic function between the width of the mine room and the critical safe height of the goaf. As the width of the mine room increases, the critical safe height of the goaf decreases according to a logarithmic function with a gradually decreasing rate of decrease.
3. The highest correlation coefficient between the rock compressive strength and the critical safety height of the goaf was 0.98765 for the power function fit, that is, following a power function $y = a_3 x^{b_3}$, in which a_3 and b_3 mainly depend on the rock compressive strength and other factors. Figure 3c shows the rock body compressive strength and the critical safe height of the goaf power function fitting curve. As the rock body compressive strength increases, the critical safe height of the goaf increases gradually according to a power function, with the rate of increase gradually increasing.
4. The highest correlation coefficient between the width of the mine pillar and the critical safety height of the goaf function fit as the logarithmic function fit of 0.99999, that is, following the logarithmic function $y = a_4 - b_4 \ln(x + c_4)$ of the incremental law (where a_4 , b_4 , and c_4 mainly depend on the width of the mine pillar, the rock body compressive strength, and other factors). Figure 3d shows the logarithmic function fitting curve of the mine pillar width and critical safety height of the goaf. As the mine pillar width increases, the critical safe height of the goaf increases gradually according to a logarithmic function, with the rate of increase gradually increasing.
5. The highest correlation coefficient of the function fit between the mining height and the critical safety height of the goaf was 0.98822, following a decreasing linear function of the form $y = a_5 + b_5 x$ (in which a_5 and b_5 mainly depend on the mining height and other factors). Figure 3e shows the fitting curve of the logarithmic function between the mining height and the critical safe height of the goaf. As the mining height increases, the critical safe height of the goaf decreases linearly.

3.3. Theoretical Analysis of Project Examples

The results in Table 2 show a large gap between the results of rock body compressive strength discounting in different areas of the mine. The mine is strictly in accordance with the established structural parameters, i.e., the one-step mining room being 12 m, the two-step mining pillar being 18 m divided into blocks, and the existing middle section of the division of the stopes being carried out in accordance with engineering construction specifications. Therefore, the critical safe height of the goaf depends only on the rock body compressive strength and the mining height. The calculation results are shown in Figure 4.

According to the results shown in Figure 4a, in the section with poor stability, when the design mining height is in the range of 10–70 m, the critical safe height of the goaf is between 20 and 30 m. When the design mining height is 25 m, the critical safe heights of the goaf are 29.08 m (−378 m middle section) and 27.84 m (−478 m middle section). When the design mining height is 30 m, the critical safe heights of the goaf are 28.63 m (−378 m middle section) and 27.41 m (−478 m middle section). Therefore, in order to achieve higher recycling efficiency with the goal of guaranteeing safety, the height of the stope should not exceed 28 m (in the −378 m middle section) or 27 m (in the −478 m middle section).

According to the results shown in Figure 4b, for the section with better stability, when the design mining height is in the range of 10–70 m, the critical safe height of the goaf is between 45 and 65 m. When the design mining height is 50 m, the critical safe heights of the goaf are 55.43 m (−378 m middle section) and 53.08 m (−478 m middle section). When the design mining height is 55 m, the critical safe heights of the stope are 54.11 m (−378 m middle section) and 51.82 m (−478 m middle section). Therefore, in order to achieve higher recovery efficiency with the goal of guaranteeing safety, the heights of the goaf should not exceed 54 m (−378 m middle section) and 51 m (−478 m middle section).

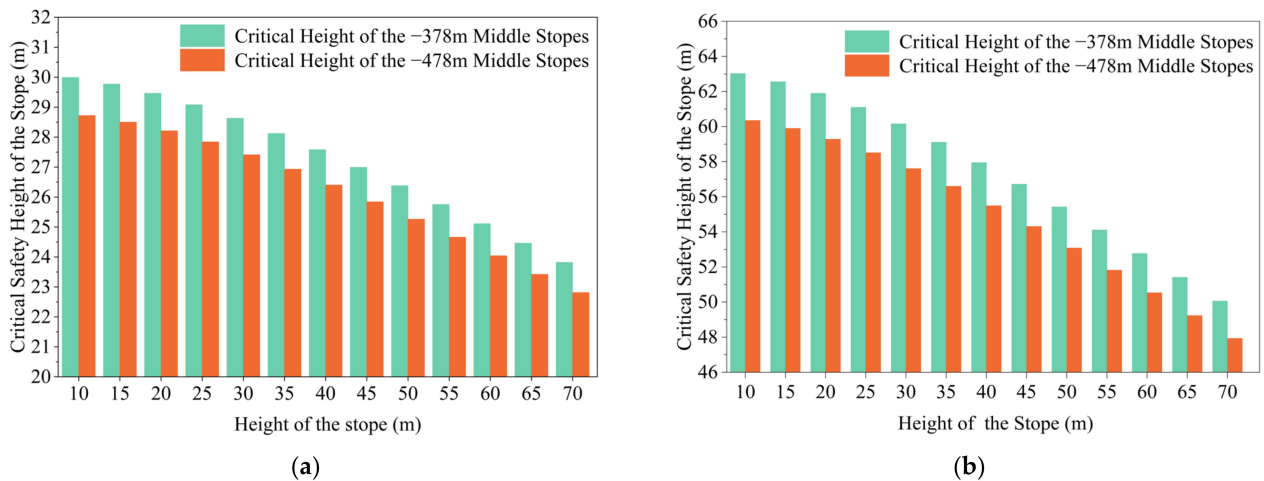


Figure 4. Correspondence between the design mining height and mining depth of stopes in different regions and the safety critical height of goaf. (a) Correspondence between the design mining height of the stopes and the safety critical height of the goaf in the area of poor rock stability in the middle section of -378 m and the middle section of -478 m; (b) Correspondence between the design mining height of the stopes and the safety critical height of the goaf in the area of better rock stability in the middle section of -378 m and the middle section of -478 m.

3.4. Numerical Simulation Testing of Project Examples

The analysis of the results is aimed at the empty field state in which the back mining of the one-step mining room is completed and unfilled. Figure 5 shows maps of the stress and displacement during the mining process obtained by taking the example of the mining site in the area with better rock stability and the designed height of the mining site of 50 m; the mining site in the area with poorer rock stability and the designed height of the mining site of 30 m. The maximum compressive stress, maximum tensile stress, maximum displacement, and maximum compressive stress safety coefficient within the roof and sidewall (two-step mining pillars) of the one-step mining room were counted in Figure 6 under different simulation scenarios, respectively.

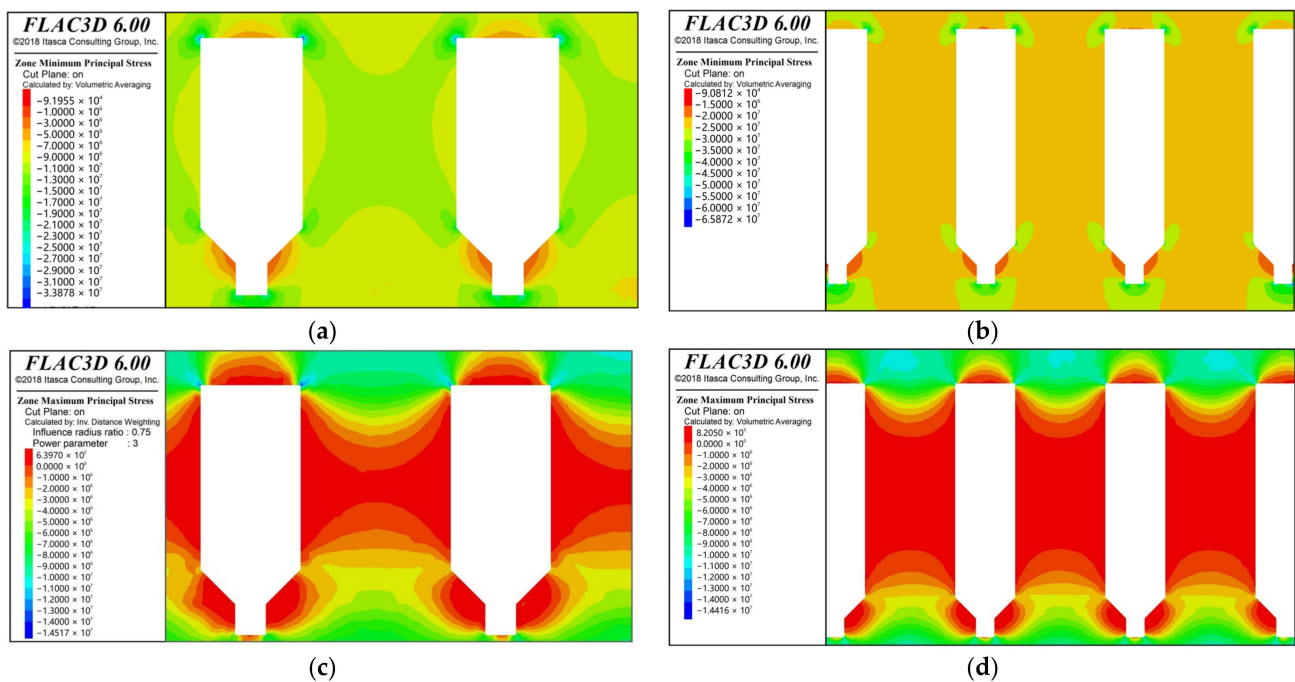


Figure 5. Cont.

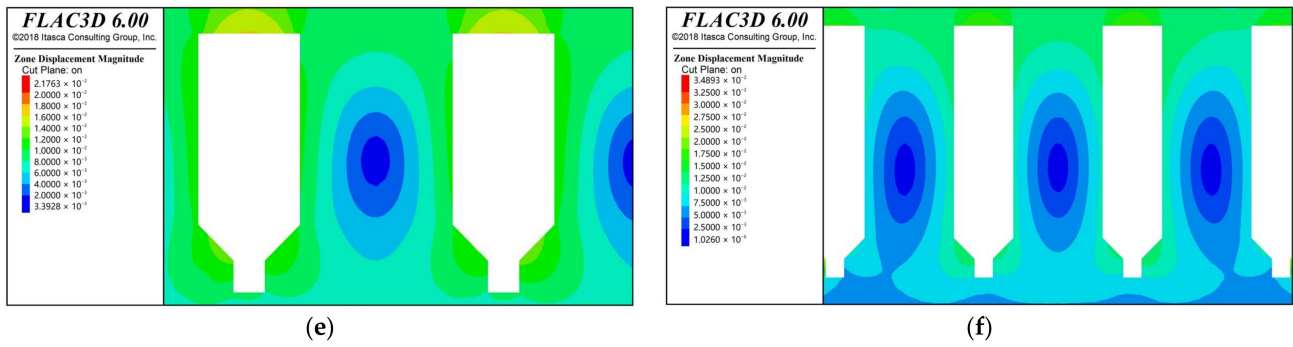


Figure 5. Stress and displacement maps of the mining process. (a) Compressive stress cloud at 30 m height of the goaf; (b) Compressive stress cloud at 50 m height of the goaf; (c) Tensile stress cloud at 30 m height of the goaf; (d) Tensile stress cloud at 50 m height of the goaf; (e) Displacement cloud at 30 m height of the goaf; (f) Displacement cloud at 50 m height of the goaf.

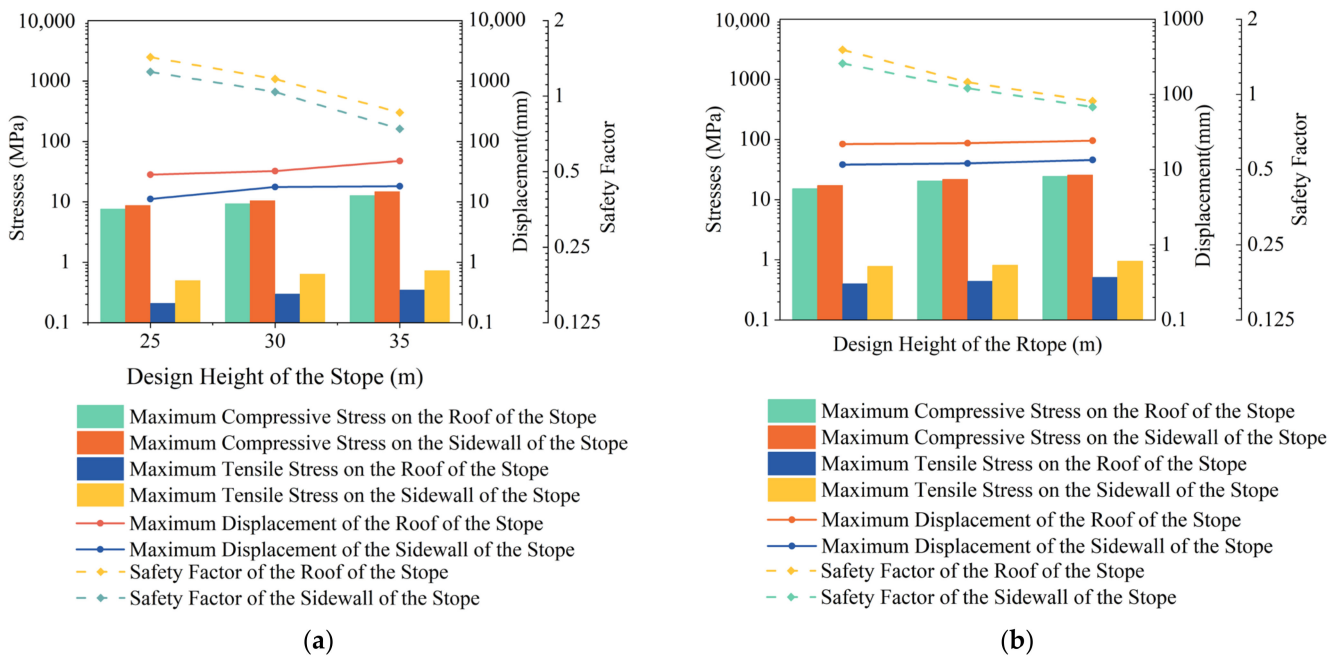


Figure 6. Trends in the results of the numerical simulation schemes. (a) Trends in stress, displacement and factor of safety in areas of poor rock stability; (b) Trends in stress, displacement and factor of safety in areas of better rock stability.

3.4.1. Compressive Stress Analysis

From Figures 5a,b and 6a, it can be seen that the compressive stress distribution of both the roof of the goaf and the sidewall are wider, and the values are generally larger. This is due to the stress release at the mining location after mining back and the stress concentration in the surrounding rock around the mining area. It is worth noting that the stress concentration phenomenon occurs at the junction of two or three faces. Therefore, the corners of the goaf in the actual mining process are generally curved instead of forming a right angle as in the design.

Under the conditions of the same rock stability level and the same height of the goaf, the pressure of the sidewall in the goaf is slightly larger than the pressure of the roof, but the difference is not large. For example, in the area of poor rock stability, under the condition that the height of the stope is 30 m, and the maximum compressive stresses of the side gang and the roof plate are 10.51 MPa and 9.36 MPa, respectively. Under the condition of the same rock stability level, as the height of the goaf increases, the compressive stresses on the roof plate and sidewalls of the goaf increase gradually. For example, in the area of

poor stability, when the height of the goaf is increased from 25 m to 35 m, the maximum compressive stress of the roof plate of the goaf is increased from 7.65 MPa to 12.77 MPa, and the maximum compressive stress of the sidewalls is increased from 8.74 MPa to 14.85 MPa. Therefore, when the stability of the surrounding rock is poor, it is appropriate to reduce the height of the goaf to ensure the safety of the back mining.

3.4.2. Tensile Stress Analysis

From Figures 5a,b and 6b, it can be seen that the tensile stresses on the roof and sidewalls of the goaf are distributed over a wide range and that the maximum tensile stresses on the sidewalls run through the entire two-step pillar. On the one hand, the tensile stress is dispersed from the center of the pillar to the left and right sides in a symmetric trumpet shape, and the magnitude of the tensile stress is unchanged. On the other hand, it decreases gradually from the center of the pillar to the upper and lower ends and decreases gradually.

For a given rock stability level and mining height, the tensile stress of the sidewalls in the mining area is slightly larger than that of the roof, but they are not very different. For example, in the better stability area, the maximum tensile stresses of the sidewalls and top plate are 0.82 MPa and 0.84 MPa, respectively, when the height of the stope is 50 m.

For the same rock stability grading conditions, as the height of the stope increases, the tensile stresses on the roof plate and sidewall of the goaf are gradually increased. For example, in the area of better rock stability, when the height of the stope increases from 45 m to 55 m, the maximum tensile stress of the roof plate of the stope increases from 0.4 MPa to 0.51 MPa, and the maximum tensile stress of the sidewall increases from 0.78 MPa to 0.95 MPa. Thus, at greater goaf heights, the tensile stresses of the rock around the mining area are much smaller than the ultimate tensile strength of the rock. Therefore, the maximum compressive stress should be mainly considered in assessing the potential for extrusion damage to the top plate and sidewall.

3.4.3. Displacement Analysis

Figure 6a,b show that the displacements of the roof plate and sidewalls of the stope have large distribution ranges, mainly concentrated in the upper part of the mined area, with a funnel-shaped distribution. In particular, the maximum displacement generally occurs in the top plate of the mining hollow area, mainly due to the loss of support for the top plate in the hollow area, which ultimately makes the top plate appear larger deformation, and the side gang deformation is smaller.

Under the same rock stability grading conditions, as the height of the stope increases, the displacement of the roof plate of the stope gradually increases. For example, in the area of poor stability, when the height of the stope increases from 25 m to 35 m, the maximum displacement of the roof plate of the stope increases from 28.23 mm to 47.52 mm. In the area of good stability, when the height of the stope increases from 45 m to 55 m, the maximum displacement of the roof plate of the stope increases from 21.85 mm to 24.36 mm. It is worth noting that the maximum displacement of the stope roof in the less stable area is greater than the maximum displacement of the stope roof in the more stable area. The goaf roof displacement is strongly influenced by the rock stability level.

In summary, although the height of the stope and the stability of the regional rock body in the tensile stress have a certain impact on the roof of the stope and the sidewall, they are not beyond the ultimate tensile strength of the rock body. In terms of displacement, the main influence is the deformation of the roof of the stope; the amount of deformation is relatively small. Therefore, in order to determine the reasonable height of the stope accurately, it is also necessary to determine the maximum compressive stress safety coefficient from the goaf roof and sidewall. As Figure 6a,b show, when the rock stability is poor, the height of the stope is 30 m. The roof plate and sidewall safety coefficients are 1.17 and 1.04, so the height of the stope in this section should not be more than 30 m. In the region of good rock

stability, the height of the stope is 50 m, and the top plate and sidewall safety coefficients are 1.12 and 1.06, so the height of the stope in the section should not be more than 50 m.

4. Industrial Tests

4.1. Overview of the Experimental Stope

Three stopes, numbered 1, 2, and 3, were selected for industrial testing. The #1 test stope was located between exploration lines 4 and 5 of the N1 ore body in the middle section of -478 m, the #2 test stope was located between exploration lines 6 and 7 of the N3 ore body in the middle section of -378 m, and the #3 test stope was located between exploration lines 8 and 9 of the S1 ore body in the middle section of -378 m. The field investigation and rock stability evaluation results show that the #1 test stope and #2 test stope area rock body is poor and stability is poor; the #3 test stope area rock body is better.

Each test stope adopts the method of filling the empty field after the rock drilling stage, and does not change the width of the one-step mining room and the two-step mining pillar. The length of the stope is arranged according to the standard stope. However, according to the different geological conditions and mining conditions of the areas where the test stopes are located, different heights of the stopes are designed. Specifically, the height of the #1 test stope was 25 m, the height of the #2 test stope was 30 m, and the height of the #3 test stope was 50 m.

4.2. Results of Industrial Experiments

Immediately after the completion of the last ore discharge from each test stope, the GOSLAM RS100 scanner was used to scan the voided area, a 3D voided area scanning model was established, and the scanning boundary profile of the voided area was plotted, as shown in Figure 7. In order to more intuitively reflect the collapse of the hollow zone, the volume of the hollow zone was compared with the design volume, as shown in Table 6.

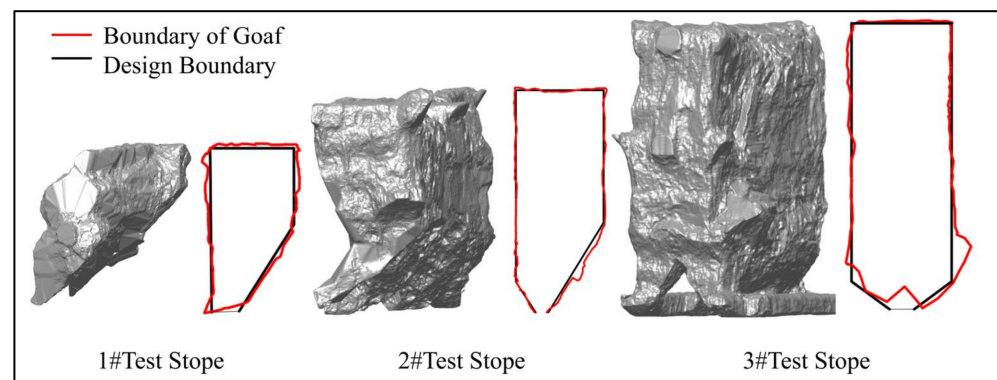


Figure 7. Goaf model and boundary profile.

Table 6. Statistical analysis of empty space volume in test stope.

Test Stope	Design Parameters of the Stope			Volume (V_1/m^3)	Volume of the 3D Model of the Goaf (V_2/m^3)	Deviation Factor * ($f/\%$)
	Length (m)	Width (m)	Height (m)			
1#	50	12	25	12,511	12,787	2.21
2#	50	12	30	15,405.5	15,752	2.25
3#	50	12	50	27,292.5	27,665.5	1.37

Note: Deviation Factor * $f = \frac{V_2 - V_1}{V_1} \times 100\%$. If the stope deviation "f" factor is "+", it indicates that the goaf is generally over-excavated; conversely, if the goaf deviation factor "f" is "-", it indicates that the stope is generally under-excavated.

The over-excavation amounts for test stopes 1, 2, and 3 were 2.21%, 2.25%, and 1.37%, respectively, which are relatively small amounts. The over-excavation was mainly concentrated in the corners of the roof slab of the mining area and the bottom structure

of the stope, which may be affected by many factors such as stress concentration, skewed boreholes, fault development, poor charging accuracy, and blasting construction. The actual mining operation in the two-step mining room increases the difficulty of retaining the shoring wall pillars, the ore depletion rate, and the difficulty of constructing the mine access road.

On the whole, the actual boundaries of the three test stopes under the empty field condition are basically consistent with the design boundaries, and there is no obvious instability and collapse phenomenon. The industrial test results show that the mine does not change the one-step and two-step width of the stope according to the stability of the regional rock body and mining depth. The height of the stopes, adjusted for the stope safety below the critical height of the stope, can effectively reduce the phenomenon of instability and collapse of the stope. Specifically, in the middle section of -378 m, the height of the stope in the area of better rock stability is 50 m, and the height of the stope in the area of poorer rock stability is 30 m; in the middle section of -478 m, the height of the stope in the area of better rock stability is 50 m, and the height of the stope in the area of poor rock stability is 25 m.

5. Conclusions

In this study, a formula for the safe critical goaf height for the stage airfield filling mining method was derived based on rock body strength discounting, Pu's arch equilibrium theory, and the ultimate strength formula of the Bieniawski pillar. The main influencing factors were analyzed by means of an extreme quadrature experiment. In addition, the reliability of the theoretical calculation results was verified by numerical simulation tests and industrial tests. Based on this study, the following conclusions can be drawn.

- (1) According to a comprehensive analysis of polar-orthogonal experiments, among the main factors affecting the critical safety height of the goaf, the impact of the compressive strength of the rock body is the most significant; followed by the width of the two-step mining pillar; and finally, the height of the stope, the depth of mining, and the width of the one-step mining room, the effect of which are almost the same. The effects of the mining depth, the width of the one-step mining room, and the critical safe height of the goaf follow decreasing logarithmic functions; the effects of the compressive strength of the rock body and the critical safe height of the goaf follow increasing power functions; the effects of the width of the two-step mining pillar and the critical safe height of the goaf follow increasing logarithmic functions; and the height of the goaf and the critical safe height of the goaf follow decreasing linear functions.
- (2) Based on the geological conditions of the mine and the current mining situation, the permissible critical height of mining safety was calculated for each area of the mine. The calculation results show that: in the area with poor rock stability, the heights of the stope should not exceed 28 m (-378 m middle section) and 27 m (-478 m middle section); in the area with better rock stability, the heights of the stope should not exceed 54 m (-378 m middle section) and 51 m (-478 m middle section).
- (3) Numerical simulation tests were carried out using FLAC 3D, and the results show that the stope is significantly affected by compressive stress and increases with increasing stope height; the tensile stress does not exceed the ultimate tensile strength of the rock body; and the displacement and deformation are relatively small and do not exhibit sudden changes. In the area of poor rock stability, when the height of the stope is 25 m, 30 m, and 35 m, respectively, the safety coefficients of the roof plate in the goaf is 1.43, 1.17, and 0.86; the safety coefficients of the sidewall in the goaf is 1.25, 1.04, and 0.74. In the area of better rock stability, when the height of the stope is 45 m, 50 m, and 55 m, respectively, the safety coefficients f of the roof plate in the goaf is 1.51, 1.12, and 0.94; the safety coefficients f of the r sidewall in the goaf is 1.33, 1.06, and 0.89. The former heights are slightly greater than the results suggested by the theoretical calculations, and the latter are basically the same as the theoretical calculation results.

- (4) The industrial test results show that the three test stopes are in a state of over-excavation but that the amount of over-excavation is relatively small, within the range of 1%–3%. The actual boundary of the open area is relatively regular and is basically consistent with the design boundary. On the whole, the boundary meets the basic requirements of safe production and does not affect two-step pillar mining.

The method provides a reference and a practical basis for determining a reasonable stage height in similar metal mines using the empty-space subsequent filling mining method. It is worth noting that the stope length does not contribute to the use of the formula in the empty-space subsequent filling mining method. Therefore, in the future, the stope length can be included as a key factor in the formula to adapt to different mining methods. Meanwhile, in addition to the influencing factors considered in this study, with the increase of the mining depth, the change of the plastic zone in the upper part of the goaf, the effect of the backfilling body or goaf group in the upper part of the goaf, and the vibrational inertial force generated by the blasting vibration on the stability of the goaf are the main aspects to be considered to improve its accuracy and predictive ability.

Author Contributions: Writing—original draft preparation, Q.Z. and P.Z.; data curation, P.Z. and H.L. conceptualization, Q.Z. and P.Z.; methodology, Q.C., H.L. and Z.S.; software, Q.Z., Z.S. and Y.T.; validation, P.Z. and Q.C.; writing—review and editing, Q.Z. and P.Z.; supervision, Q.C.; funding acquisition, Q.Z. All authors have read and agreed to the published version of the manuscript.

Funding: This research was funded by the National Natural Science Foundation of China grant number 52274151 the Science and Technology Innovation Program of Hunan Province grant number 2021RC3125, and the APC was funded by Qiusong Chen.

Data Availability Statement: All data are shown in the article.

Acknowledgments: The authors also would like to thank Jiaduo Ding, and Zhiyue Lin for their support with industrial tests during the research process.

Conflicts of Interest: Author H.L. was employed by the Jiangxi Copper Industry Group Yinshan Mining Industry Co., Ltd. The remaining authors declare that the research was conducted in the absence of any commercial or financial relationships that could be construed as a potential conflict of interest.

References

1. Chen, Q.; Zhou, H.; Wang, Y.; Wang, D.; Zhang, Q.; Liu, Y. Erosion wear at the bend of pipe during tailings slurry transportation: Numerical study considering inlet velocity, particle size and bend angle. *Int. J. Miner. Metall. Mater.* **2023**, *30*, 1608–1620. [[CrossRef](#)]
2. Guo, L.; Wu, Y.; Zhang, Q.; Chen, Q. Stability evaluation of layered backfill considering filling interval, backfill strength and creep behavior. *Minerals* **2022**, *12*, 271. [[CrossRef](#)]
3. Liu, Y.; Wang, Y.; Chen, Q. Using cemented paste backfill to tackle the phosphogypsum stockpile in china: A down-to-earth technology with new vitalities in pollutants retention and CO₂ abatement. *Int. J. Miner. Metall. Mater.* **2023**. Available online: <http://ijmmm.ustb.edu.cn/en/article/id/e87e96bf-4935-4a0f-bbf2-0033535b0b9b> (accessed on 1 December 2023).
4. Liu, Y.; Molinari, S.; Dalconi, M.C.; Valentini, L.; Bellotto, M.P.; Ferrari, G.; Pellay, R.; Rilievo, G.; Vianello, F.; Salviulo, G.; et al. Mechanistic insights into pb and sulfates retention in ordinary portland cement and aluminous cement: Assessing the contributions from binders and solid waste. *Hazard. Mater.* **2023**, *458*, 131849. [[CrossRef](#)]
5. Wang, R.; Zeng, F.; Li, L. Stability analyses of side-exposed backfill considering mine depth and extraction of adjacent stope. *Int. J. Rock. Mech. Min. Sci.* **2021**, *142*, 104735. [[CrossRef](#)]
6. Qi, C.; Wu, M.; Liu, H.; Liang, Y.; Liu, X.; Lin, Z. Machine learning exploration of the mobility and environmental assessment of toxic elements in mining-associated solid wastes. *J. Clean. Prod.* **2023**, *401*, 136771. [[CrossRef](#)]
7. Wu, M.; Qi, C.; Derrible, S.; Choi, Y.; Fourie, A.; Ok, Y.S. Regional and global hotspots of arsenic contamination of topsoil identified by deep learning. *Commun. Earth Environ.* **2024**, *5*, 10. [[CrossRef](#)]
8. Yuan-hui, L.; Gang, L.; Shi-da, X.; Da-wei, W. The spatial-temporal evolution law of microseismic activities in the failure process of deep rock masses. *J. Appl. Geophys.* **2018**, *154*, 1–10. [[CrossRef](#)]
9. Golik, V.I.; Klyuev, R.V.; Martyushev, N.V.; Kondratiev, V.V.; Tynchenko, V.S.; Gladkikh, V.A.; Iushkova, L.V.; Brigida, V. Reuse and Mechanochemical Processing of Ore Dressing Tailings Used for Extracting Pb and Zn. *Materials* **2023**, *16*, 7004. [[CrossRef](#)] [[PubMed](#)]

10. Uzarowicz, Ł.; Wolińska, A.; Błomska, E.; Szafranek-Nakoneczna, A.; Kuźniar, A.; Ślodziak, Z.; Kwasowski, W. Technogenic soils (technosols) developed from mine spoils containing Fe sulphides: Microbiological activity as an indicator of soil development following land reclamation. *Appl. Soil. Ecol.* **2020**, *156*, 103699. [[CrossRef](#)]
11. Kongar-Syuryun, C.B.; Kovalski, E.R. Hardening backfill at potash mines: Promising materials regulating stress-strain behavior of rock mass. *Geol. I Geofiz. Yuga Ross. Geol. Geophys. Russ. South.* **2023**, *13*, 177–187. [[CrossRef](#)]
12. Kovalski, E.R.; Kongar-Syuryun, C.B.; Petrov, D.N. Challenges and prospects for several-stage stoping in potash mining. *Sustain. Dev. Mt. Territ.* **2023**, *15*, 349–364. [[CrossRef](#)]
13. Khayrutdinov, M.M.; Golik, V.I.; Aleksakhin, A.V.; Trushina, E.V.; Lazareva, N.V.; Aleksakhina, Y.V. Proposal of an Algorithm for Choice of a Development System for Operational and Environmental Safety in Mining. *Resources* **2022**, *11*, 88. [[CrossRef](#)]
14. Ganapathy, G.P.; Zaalishvili, V.B.; Chandrasekaran, S.S.; Melkov, D.A. Integrated monitoring of slope process in India and Russia. *Sustain. Dev. Mt. Territ.* **2020**, *12*, 572–581. [[CrossRef](#)]
15. Driouch, A.; Ouadif, L.; Lahmili, A.; Belmi, M.A.; Benjmel, K. Geotechnical modeling of the method for mining cobalt deposits at the Bou Azzer Mine, Morocco. *Min. Miner. Depos.* **2023**, *17*, 51–58. [[CrossRef](#)]
16. Obert, L.; Duvall, W.I. *Rock Mechanics and Design of Structures in Rock*; John Wiley & Sons: New York, NY, USA, 1967.
17. Jiang, L.; Yang, C.; Jiao, H. Ultimately exposed roof area prediction of bauxite deposit goaf based on macro joint damage. *Int. J. Min. Sci. Technol.* **2020**, *30*, 699–704. [[CrossRef](#)]
18. Swift, G.; Reddish, D. Stability problems associated with an abandoned ironstone mine. *Bull. Eng. Geol. Environ.* **2002**, *6*, 227–239. [[CrossRef](#)]
19. Peng, G.; Gaoyi, D.; Jingsong, C.; Zhou, C.; Manqing, L.; Weizhong, Z.; Yang, S. Study on optimization of stope structural parameters and filling scheme of wawu phosphate mine in yichang city, china. *Front. Earth Sci.* **2022**, *10*, 883572. [[CrossRef](#)]
20. Zhienbayev, A.; Balpanova, M.; Asanova, Z.; Zharaspaev, M.; Nurkasyn, R.; Zhakupov, B. Analysis of the roof span stability in terms of room-and-pillar system of ore deposit mining. *Min. Miner. Depos.* **2023**, *17*, 129–137. [[CrossRef](#)]
21. Hosseini, M.; Azhari, A.; Lotfi, R.; Baghbanan, A. Safety analysis of Sormeh underground mine to improve sublevel stoping stability. *Deep. Undergr. Sci. Eng.* **2023**, *2*, 173–187. [[CrossRef](#)]
22. Bagde, M.; Sangode, A.; Jhanwar, J. Evaluation of Stopping Parameters through Instrumentation and Numerical Modelling in Manganese Mine in India: A Case Study. *Procedia Eng.* **2017**, *191*, 10–19. [[CrossRef](#)]
23. Soni, A.; Monsalve, J.J.; Bishop, R.; Ripepi, N. Modified design of pillar based on estimated stresses and strength of pillar in an underground limestone mine. *Min. Metall. Explor.* **2023**, *40*, 529–541. [[CrossRef](#)]
24. Zhang, Y.F.; Ni, P.P. Design optimization of room and pillar mines: A case study of the xianglushan tungsten mine. *Q. J. Eng. Geol. Hydrogeol.* **2018**, *51*, 352–364. [[CrossRef](#)]
25. Qiu, H.Y.; Huang, M.Q.; Weng, Y.-J. Stability evaluation and structural parameters optimization of stope based on area bearing theory. *Minerals* **2022**, *12*, 808. [[CrossRef](#)]
26. Bieniawski, Z.T. A method Revisited: Coal Pillar Strength Formula Based on Field Investigations. In *Proceedings of the Workshop on Coal Pillar Mechanics and Design*; US Department of the Interior, US Bureau of Mines: Washington, DC, USA, 1992; pp. 158–165.
27. Fan, H.; Li, L.; Liu, H.; Hu, J.; Zhang, M.; Zhou, S.; Yang, G. Improvement to the calculating model of the pressure arch's height considering the confining pressure in the excavation of shallow tunnels. *Arab. J. Geosci.* **2021**, *14*, 1130. [[CrossRef](#)]
28. Kastner, H. *Statik des Tunnel-Und Stollenbaues auf Der Grundlagen Geomechanischer Erkenntnisse*; Springer: Berlin/Heidelberg, Germany, 2013.
29. Tu, H.; Zhou, H.; Lu, J.; Gao, Y.; Shi, L. Elastoplastic coupling analysis of high-strength concrete based on tests and the Mohr-Coulomb criterion. *Constr. Build. Mater.* **2020**, *255*, 119375. [[CrossRef](#)]
30. Zhang, J.; Wang, Z.; Song, Z. Numerical study on movement of dynamic strata in combined open-pit and underground mining based on similar material simulation experiment. *Arab. J. Geosci.* **2020**, *13*, 785. [[CrossRef](#)]
31. Liu, B.; Zhou, J.; Wen, X.; Guo, J.; Deng, Z.; Hu, X. Mechanical performance and failure criterion of coral concrete under combined compression-shear stresses. *Constr. Build. Mater.* **2021**, *288*, 123050. [[CrossRef](#)]
32. Wang, J.; Ren, L.; Xie, L.Z.; Xie, H.P.; Ai, T. Maximum mean principal stress criterion for three-dimensional brittle fracture. *Int. J. Solids Struct.* **2016**, *102–103*, 142–154. [[CrossRef](#)]

Disclaimer/Publisher's Note: The statements, opinions and data contained in all publications are solely those of the individual author(s) and contributor(s) and not of MDPI and/or the editor(s). MDPI and/or the editor(s) disclaim responsibility for any injury to people or property resulting from any ideas, methods, instructions or products referred to in the content.